C. R. Mecanique 340 (2012) 917–932

Contents lists available at SciVerse ScienceDirect

Comptes Rendus Mecanique

www.sciencedirect.com

Out of Equilibrium Dynamics

Large Eddy Simulation of turbulent flames in a Trapped Vortex Combustor (TVC) – A flamelet presumed-pdf closure preserving laminar flame speed

Cindy Merlin, Pascale Domingo, Luc Vervisch *

CORIA – CNRS and INSA de Rouen, technopole du Madrillet, BP 8, 76801 Saint-Etienne-du-Rouvray, France

ARTICLE INFO

Article history:
Available online 15 November 2012

Keywords:
Turbulent combustion
Large Eddy Simulation
Flamelet modeling

ABSTRACT

Flow and flame dynamics inside a trapped vortex combustor are analyzed from Large Eddy Simulation (LES) results compared against measurements. The Navier–Stokes equations are solved in their fully compressible form over a Cartesian grid resorting to immersed boundaries to account for the complex geometry, composed of an annular flow impacting a set of axisymmetric rods (flame holders) before interacting with a cavity. Various cases are considered, varying the main flow rate, the length of the cavity, injecting secondary-air and also adding a swirling motion. From these cases, three main cavity flow regimes emerge. The modeling of molecular diffusion in LES with presumed probability density function (pdf), as filter of premixed flamelets, is also discussed. It is shown that a dynamic correction to molecular diffusion may be computed from the pdf control parameters to ensure the correct laminar flame speed, whatever the mesh used. Finally, studying the turbulent flame evolution within the cavity in the various cases, suggests that swirling motion is mandatory to favor the global burner stability.

1. Introduction

The interaction between a main flow and a cavity has been the subject of multiple studies addressing a large variety of flow geometries [1–7]. Gas flow with cavities are usually characterized by large fluctuations of pressure, density and velocity components, sometimes followed by large flow instabilities and acoustic noise. On the other hand, flame stabilization may be mainly achieved through recirculation zones carrying burnt gases or against pilot flames, both bringing the energy for igniting the fuel/air mixture, or, in wakes behind obstacles within the low velocity zone in the vicinity of flame holders. Among wall-bounded flow geometries, a cavity provides a simple way to establish a permanent recirculation zone, vortices and turbulent structures are trapped within the cavity and a flame may thus in principal be stabilized above, or downstream of it. Obviously, the strong unsteady character of cavity flows may easily become a limitation if combustion instabilities appear. However, Trapped Vortex Combustor (TVC) have been developed with success [8], in which the flame is stabilized by a recirculation zone 'trapped' within a cavity. The main motivation is to provide a constant reservoir of burnt gases for flame stabilization; a recirculation zone which could be less sensitive to the main flow regime than the kernel of burnt gases ensuring flame stabilization in swirling burners, specifically when approaching lean blow out conditions.

The drag induced on the flow by a cavity has been thoroughly studied in the literature, it was found that the optimal cavity length in terms of drag reduction is associated with the appearance of quasi-stable vortices within the cavity [9,10], linked with a pseudo-stagnation of the shear layer at the downstream cavity corner [11,12]. On these grounds, various TVC (Trapped Vortex Combustor) have been discussed and studied [8,13,14].

* Corresponding author.
E-mail address: vervisch@coria.fr (L. Vervisch).

1631-0721/$ – see front matter
http://dx.doi.org/10.1016/j.crme.2012.10.039

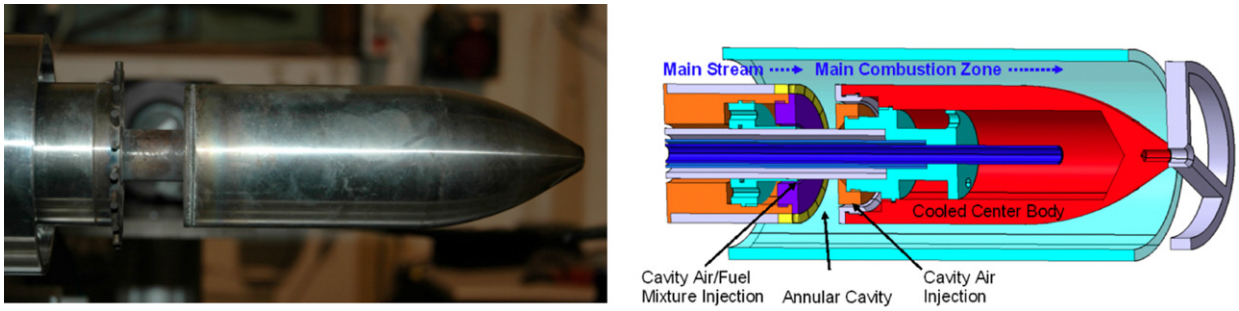

Fig. 1. Picture (left) and schematic (right) of the CORIA Trapped Vortex Combustion chamber [16].

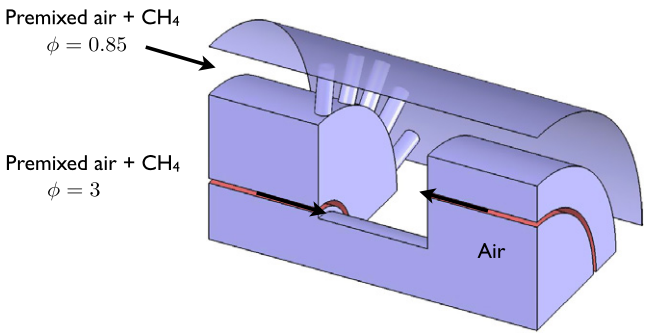

Fig. 2. Sector view of 1/4 of the combustion chamber.

Unsteady numerical modeling of an experimental setup designed in the laboratory CORIA [15,16] to study trapped vortex combustion, is reported in this article. Large Eddy Simulation is used for solving the Navier–Stokes equations in their fully compressible form. The cold flow is first analyzed, before discussing an improvement of presumed probability density function modeling for turbulent flames and simulating the reacting trapped vortex flow. The flame and flow dynamics observed in the numerical results are systematically analyzed against the available measurements. It is shown that swirling the main flow allows for strongly reducing flame oscillations, thus potentially avoiding combustion instability, which can easily develop in burner geometries featuring cavities.

2. Experimental TVC, numerics and modeling

2.1. Experiments

The studied experimental set up is composed of a main annular lean premixed methane–air flow at equivalence ratio 0.85, encountering a cavity located toward the axis of symmetric of the system (to limit the size of the full chamber, which is within a quartz cylinder allowing for optical access [15,16]). Fig. 1 shows a picture of the system without the quartz tube and a schematic of the various elements. The exit of combustion chamber is equipped with a nozzle, to operate at pressures up to 3 atmospheres, for a maximum inlet velocity of about 15 m/s. Flame holders are located right upstream of the cavity, this axisymmetric set of rods contributes to flame stability in many ways: the blockage accelerate the main flow, favor a depression above the cavity ensuring mixing between fresh gases and cavity-trapped burnt product; they also help homogenize the flow downstream of the cavity through wake turbulence, temperature in the exit plane being then more uniform.

Previous analyses have discussed the presence of two main vortex cores inside a cavity as an ingredient for flame stability [17]: burnt gases are more easily transported toward the upstream cavity wall, to be then entrained within the lower pressure zone downstream of flame holder. Another direct effect of a two vortex stable mode is the better cooling of the upper corner of the downstream cavity wall, with eventually the appearance of a recirculation zone in the vicinity of this corner. Also, to favor this two-vortex regime and feed the cavity with burnt gases, two additional annular injections are in the cavity of the CORIA TVC (Fig. 2); on the upstream wall at 1 mm of the bottom end of the cavity, a rich premixing of fuel/air mixture at equivalence ratio 3 is injected and on the downstream wall, at 2/3 of the cavity depth, air is injected inside the cavity (Figs. 1 and 2).

The flame-holder flow section is composed of 20 rods of diameter 3 mm, regularly distributed around the axis of symmetry (Fig. 2). The height of the annular main flow is 10 mm, the cavity is 19.5 mm depth and 22 mm long. The properties of the case studied, where a stable flame is observed in the experiment, are summarized in Table 1, PIV and LDV were previously conducted along with CH chemiluminescence [15,16].

Table 1
Baseline case parameters.

	Main annular flow	Rich premixed cavity	Air cavity
Air flow rate (g/s)	20	0.7	1
Equivalence ratio	0.85	3.0	0
Velocity (m/s)	8	8	6

2.2. Numerics and modeling

The simulations are performed using the SiTCom parallel flow solver [18–20], which is based on an explicit Finite Volumes (FV) scheme for Cartesian grids. The Navier–Stokes equations are solved in their fully compressible form together with scalar balance equations. The convective terms are computed resorting to a fourth-order centered skew-symmetric-like scheme [21], while the diffusive terms are computed using a fourth-order centered scheme. The 3D-NSCBC boundary conditions [22,23] are used at inlet and outlet.

Two different approaches have been used for LES; the first relies on explicit modeling of the unresolved turbulent fluxes expressed with the Vreman closure [24], a second set of calculations has been carried out with implicit Large Eddy Simulation [25], based on the fact that SGS modeling mostly plays a dissipative role in the simulations. An artificial dissipation scheme was selected [26], which introduces second and/or fourth-order dissipative terms whose global contribution is somehow similar to subgrid scale modeling [25]. Both calculations (implicit or explicit LES) need moderate second-order dissipation. However in the implicit LES, the fourth-order dissipation term is increased, to damp high frequency modes appearing in the centered scheme [27]. As these modes develop at small scales, they are naturally dissipated by the SGS model in explicit LES, then the additional fourth-order dissipative terms are not needed.

The non-dissipative skew symmetric scheme [21] is thus completed by an addition of second- and fourth-order artificial dissipation terms [28,27,26], involving an additional numerical convective flux that is controlled by four parameters α_1, α_2, β_1 and β_2. The coefficients $\alpha_1 = 0.5$ and $\alpha_2 = 0.5$ are for the second-order terms, β_1 and β_2 for the fourth-order contribution [28]. α_1 controls up-winding fluxes, while α_2 pilots the switch to upwind diffusion for a threshold value of a sensor based on pressure fluctuations [26]. β_1 characterizes the strength of the fourth-order damping and $\beta_2 = 1$ is set to switch off the fourth-order damping in case of strong discontinuities. LES with explicit SGS modeling is performed with $\beta_1 = 0.032$ and β_1 is fixed at 0.3 for implicit LES. It has been verified that slightly modifying these values does not profoundly impact on results.

One quarter of the full geometry is computed, with annular periodicity on the lateral sides of the domain. An Immersed Boundary Method [29] is used in a fully compressible formulation to represent this complex geometry on a Cartesian mesh. The computational domain is composed of $3L \times 1.9L \times 1.9L$, where L is the cavity length. The Cartesian mesh is composed of 10 853 864 cells with 43% devoted to fluid and the remaining to solid, the LES resolution in the three Cartesian directions is 188 µm $< \Delta x <$ 462 µm (streamwise) and $\Delta y = \Delta z = 209$ µm.

A transient from initial condition is computed over 8 flow-characteristic times (estimated from the bulk annular velocity and streamwise length of the computational domain), then statistics are collected over 30 characteristic times. Simulations have been performed with and without injecting synthetic turbulence [30], for comparison.

3. Cold flow analysis

In this section, air is injected through all inlets and the baseline case of Table 1 is considered. Downstream of the flame holders, the overall flow topology may be decomposed in three main parts (Fig. 3):

- In planes located between the rods, the annular flow is only weakly affected (Fig. 3(a)), with a limited penetration of the flow coming from the cavity. Behind rods, however, the wake of the flame holders strongly interacts with the cavity motion (Fig. 3(b)), leading to mixing the fluid coming from the main annular flow with the one recirculating in the cavity.
- This cavity recirculation is decomposed in two subparts: a strong recirculation zone located deep inside, with a much smaller one at the downstream bottom corner. This second vortex strongly interacts with the main flow behind rods, with a major contribution to the flushing of the cavity.
- The flow resulting from the main annular stream mixed with the cavity fluid, then impacts on the downstream corner, before it reattaches further downstream.

The streamwise velocity has been averaged in LES, in planes where PIV measurements are available [15]. The simulation captures both the quite complex flow topology and velocity amplitudes seen in the experiment (Fig. 4). This comparison against measurements is refined in Figs. 5 and 6, showing profiles of averaged and rms streamwise velocity for various x locations ($x = 0$ at the upstream cavity corner of $L = 22$ mm long). Results from the three LES procedures employed are given (SGS modeling, MILES, MILES with forced turbulence at inlet). Considering the complexity of the geometry, making

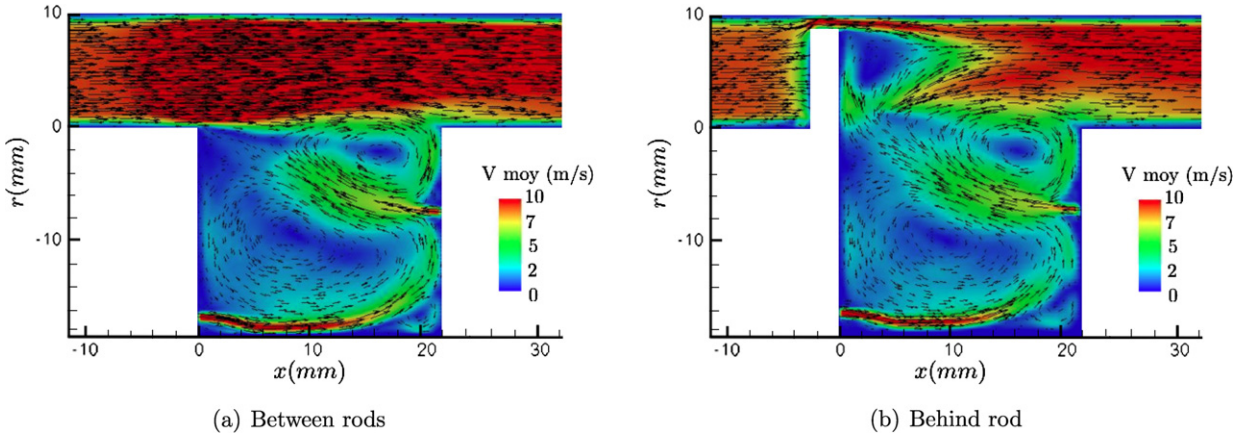

Fig. 3. In plane averaged velocity magnitude.

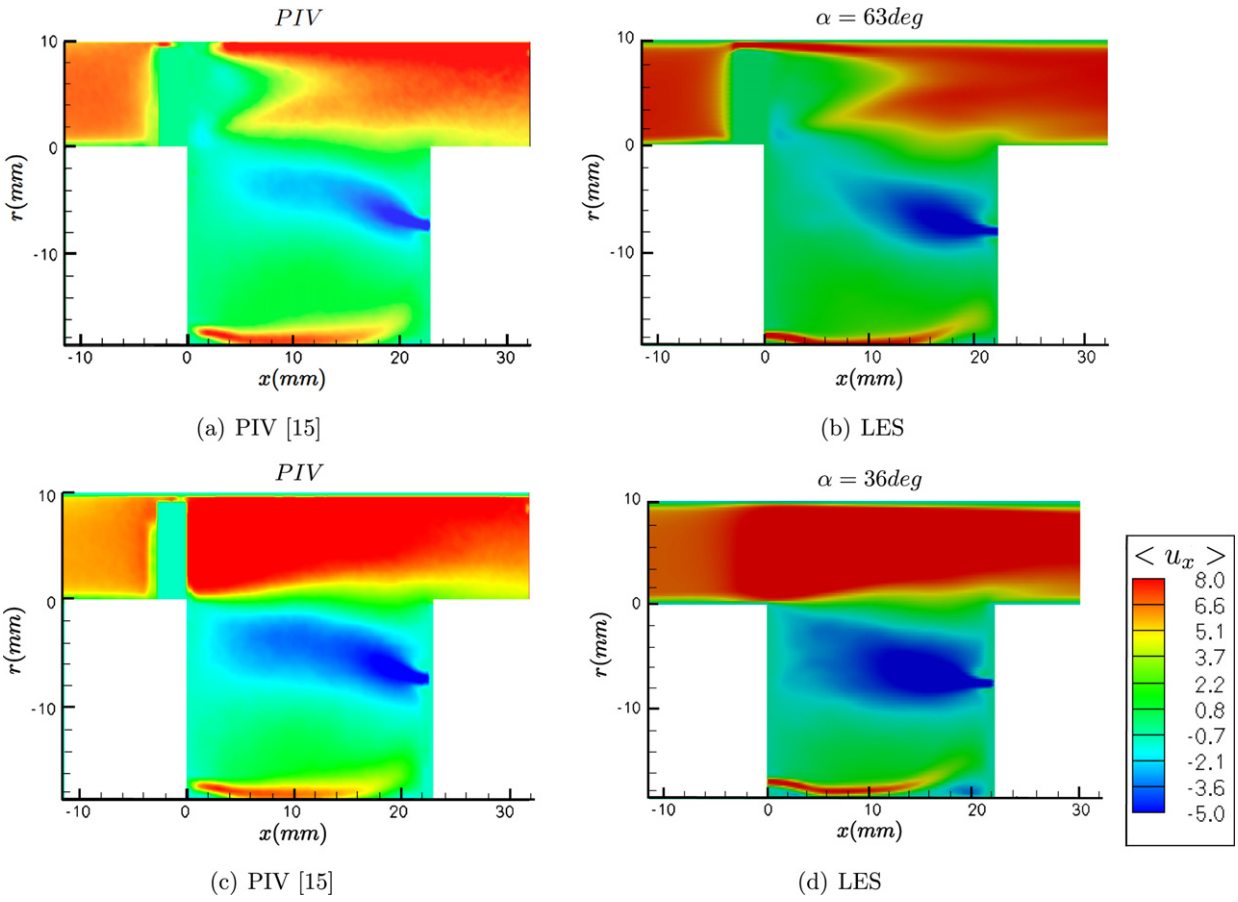

Fig. 4. Average streamwise velocity in a plane. Top: behind a rod. Bottom: between two rods.

both measurements and simulations quite challenging, the results are rather good. The mean flow is more than reasonably well captured. Moving from the cavity bottom-wall up to the annular main flow at $x = 2$ mm, Fig. 5(a) shows the secondary fuel/air injection, the almost stagnant flow inside the cavity and then the main annular flow. Further downstream, the motion inside the cavity develops, with a penetration of the cavity fuel/air jet still visible at $x = 10$ mm. The slopes of the velocity profiles in the recirculation zones are accurately captured, with however, an overestimation of the negative recirculation velocity, whatever the modeling used and this overestimation becomes larger using the SGS closure.

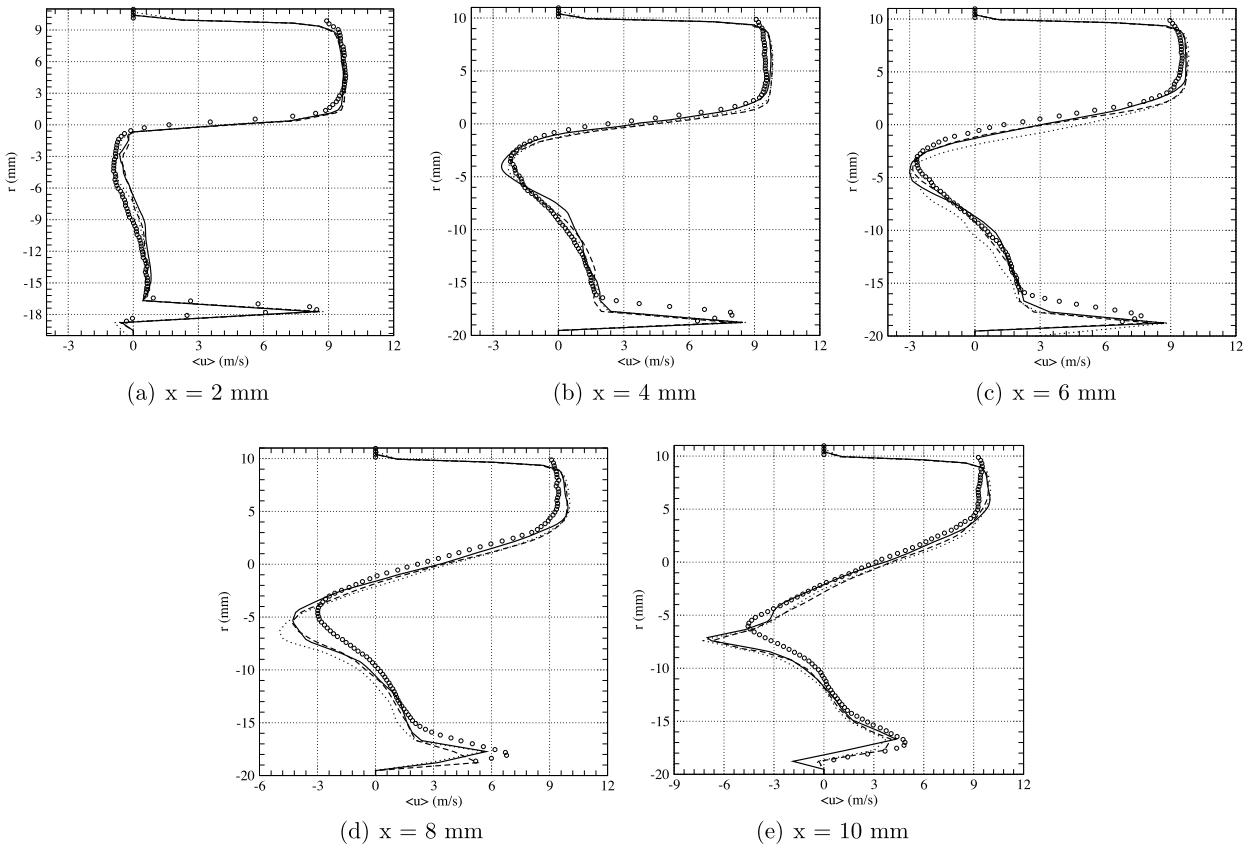

Fig. 5. Radial profiles of averaged streamwise velocity in a plane between two rods. --- MILES; — MILES with turbulence injection; ··· LES with explicit SGS closure [24]; ∘ experiments [15].

Streamwise velocity fluctuations are given in Fig. 6, overall the levels are also reproduced, with an underestimation of the secondary fuel/air jet turbulence at $x = 2$ mm, which then evolves into an over estimation downstream, except with the MILES approach bringing the results closest to experiments. This approach is thus adopted for the rest of the study.

3.1. Impact of main flow rate

From the baseline case of Table 1, the mass flow rate of the main flow, initially at 20 g/s, is varied to take the values of 10 g/s, 30 g/s and 60 g/s. Fig. 7 displays comparisons against experiments for the cases at 10 g/s and 30 g/s, the additional case at 60 g/s is investigated with the simulation only. The first of these cases (10 g/s) features similar properties in both experiment and numerical simulations. Compared to the baseline case of Fig. 3, the size of the vortical coherent structures are reduced, with the appearance of an additional recirculation zone at the leading edge of the upstream cavity corner, which ensures some mixing between the incoming flow and the cavity motions. Examining velocity fluctuations (not shown for brevity), they are lowered of about 20% compared to the reference case, but the flow is overall much less stable at large scales. Thus decreasing the flow rate below the nominal regime, may not favor stable combustion in this particular configuration.

Increasing the flow rate at 30 g/s (Fig. 7(c) and (d)) reinforces vorticity in the upper part of the cavity, to entrain more fluid inside it, as seen in both experiments and simulation in the plane behind a rod; the bottom cavity vortex is downsized in favor of the upper one, which is intensified. The mixing between the main stream and the cavity is then globally enhanced. Notice also that the sign of rotation of the vortices inside the cavity is modified with the increase of the flow rate. The maximum velocity fluctuation is up 20% compared to the baseline case. Finally, increasing the flow rate up to 60 g/s in the simulation, a single vortex is found in the cavity with more flow entrainment inside this single trapped vortex.

The axisymmetrical set of rods leads to a partial flow blockage, with acceleration followed by a pressure drop behind the rods, thus favoring mixing between the main annular stream and the fluid recirculating inside the cavity. Looking at $\langle V \rangle$, the averaged radial velocity in the vertical direction, its magnitude increases with the mass flow rate: At 10 g/s, $\langle V \rangle$ is of the order of 1.8 m/s; at 20 g/s, $\langle V \rangle \approx 4.4$ m/s; at 30 g/s, $\langle V \rangle \approx 7$ m/s and at 60 g/s, $\langle V \rangle \approx 16$ m/s (not shown for brevity).

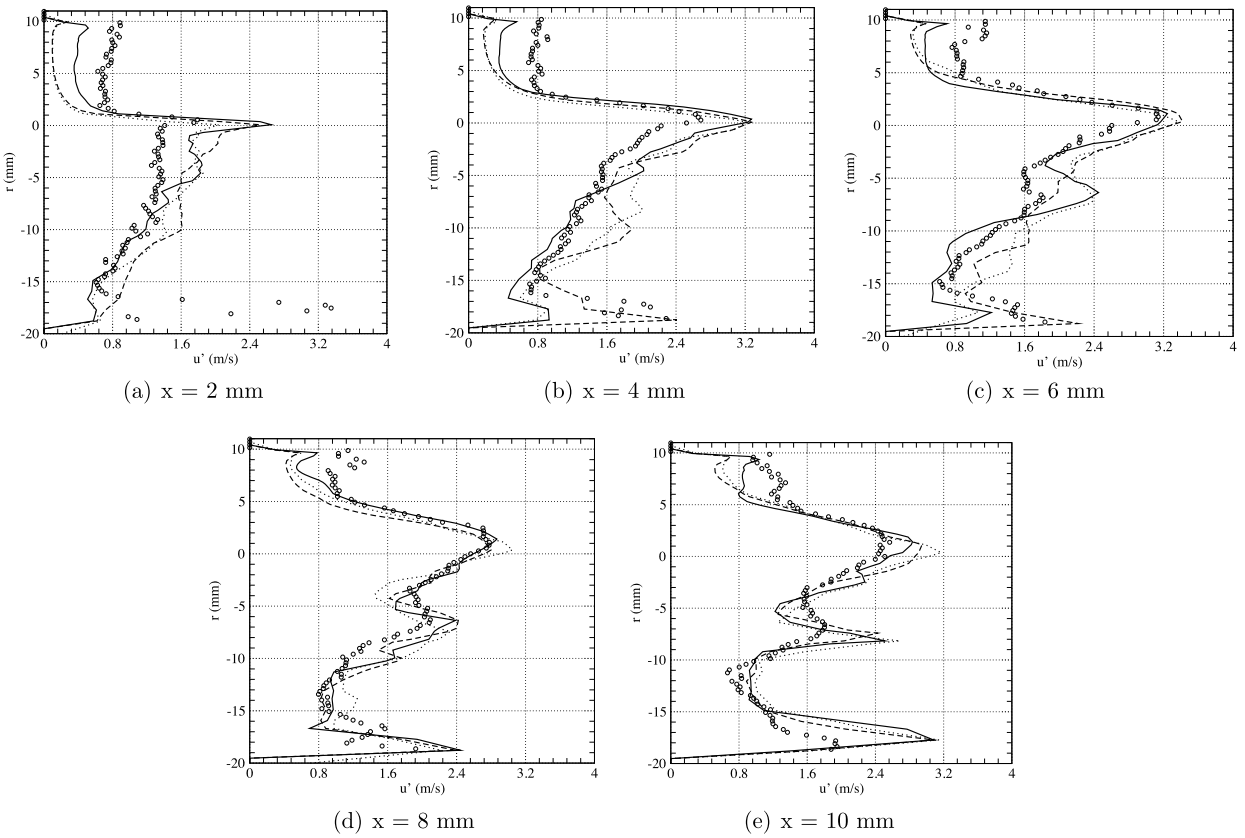

Fig. 6. Radial profiles of rms streamwise velocity in a plane between two rods. --- MILES; — MILES with turbulence injection; ··· LES with explicit SGS closure [24]; ∘ experiments [15].

Therefore, the change in main flow rate is followed by a significant enhancement of fluid exchange between the cavity and the annular flow.

3.2. Impact of cavity length and secondary-air injection

The length of the baseline case cavity is $L = 22$ mm (19.5 mm depth), it is varied to study two cavity flows with $L = 11$ mm and $L = 44$ mm, preserving the depth (Fig. 8). For $L = 11$ mm (Fig. 8(a) and (b)), the vortex above the secondary-air injection is more pronounced to fill out all of the upper part of the cavity, which is still mainly flushed through its upstream corner. The stronger interaction between the vortices and the upstream cavity wall, is followed by an increase of the velocity fluctuations, which is visible up to the main annular flow behind the flame holders. However, because of this localized intense and efficient zone of fluid exchange between the cavity and the main flow, the downstream fluctuations are lessened compared to the baseline case.

Increasing the cavity length profoundly modifies the flow patterns (Fig. 8(c) and (d)). The secondary injectors promote the development of vortices close to the bottom cavity wall, with strongly intermittent contra-rotating vortices in the upper cavity zone. Overall, increasing the length leads to less efficient mixing with the cavity and higher fluctuations in the shear layers downstream of it.

The secondary-air injection has been removed to estimate its role in the cavity flow patterns (Fig. 9). Starting from the baseline case, secondary-air in the cavity is turned off. The downstream and upper vortices are then enlarged to become the main source of connection between the cavity motion and the main flow; however, its sign of rotation is changed and the turbulence level is decreased by about 30%; confirming the key role played by this additional injection of air in trapped vortex combustor. This air-jet has a dual impact on equivalence ratio and flow structure within the cavity, bringing flammable mixture (together with its opposite jet-fuel) and favoring mixing between both main and trapped cavity flows.

3.3. Impact of swirl motion

Many fuel injection systems operate with swirling flows [31–43]. In the present burner, a swirl motion is added to the main flow with $S = 1.5$, a swirl number defined as the ratio between momentum fluxes in the azimuthal and streamwise

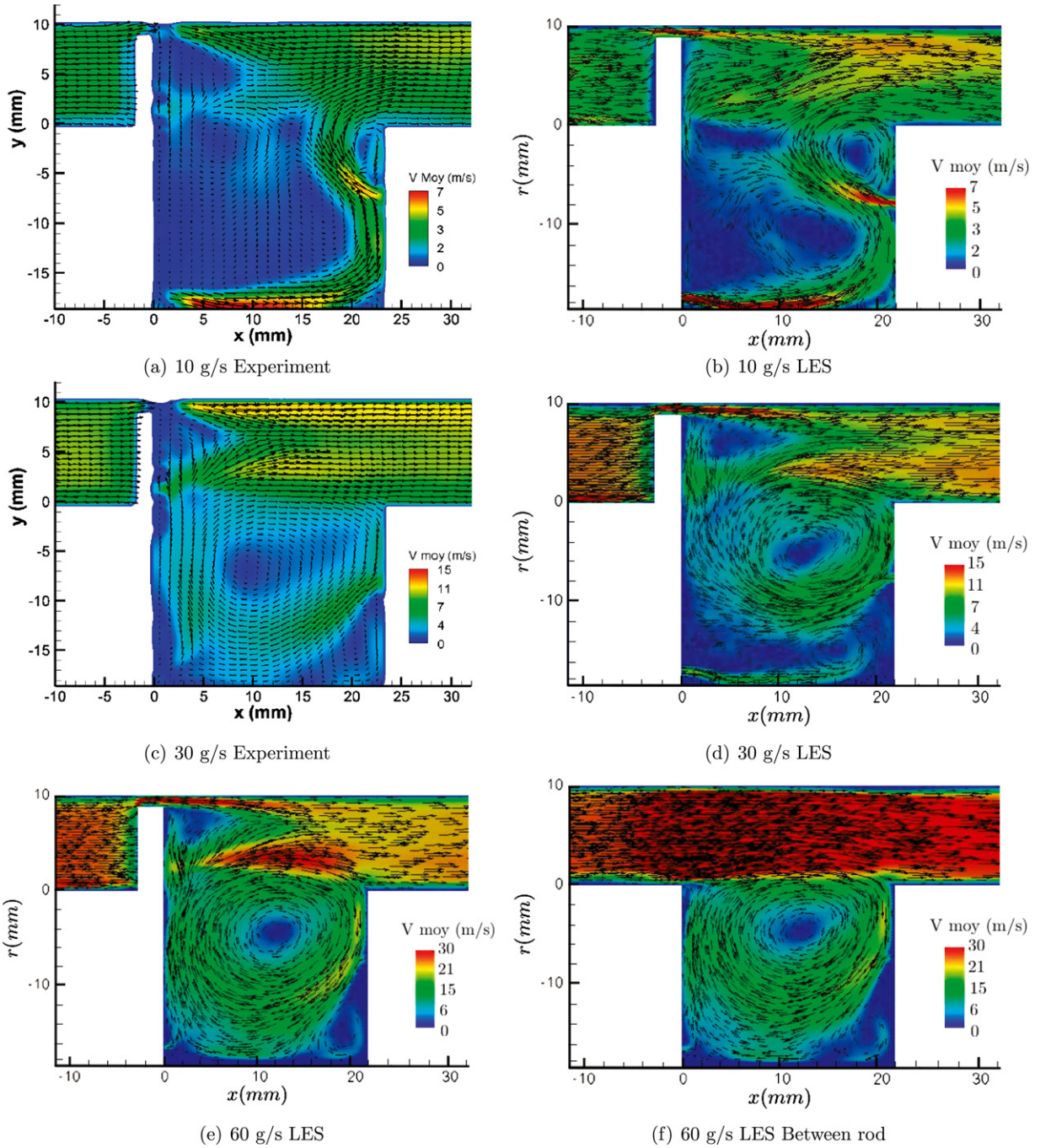

Fig. 7. Velocity magnitude for various mass flow rates.

directions. The overall impact of swirl is visible in Fig. 10, comparing the baseline case with the swirling one for a main flow rate of 30 g/s, a strong modification of the flow dynamics is seen. Two major coherent structures of same size are driving the flow within the cavity, with its emptying mainly controlled by the upper vortex. Without swirl, between rods the radial mean flow expelling fluid from the cavity is weak compared to planes behind rods, this is not the case with swirl. The shear layer topology at the merging of the main and the cavity flows, becomes much less dependent on the position considered, in the sense that almost similar flow patterns are observed in planes located either downstream of a rod (flame holder) or between two rods Fig. 11.

In summary, varying the parameters of this specific TVC burner, the flow may be classified in three main regimes (Fig. 12). For high flow rate, here about 60 g/s in the lean premixed annular flow, a single coherent structure develops

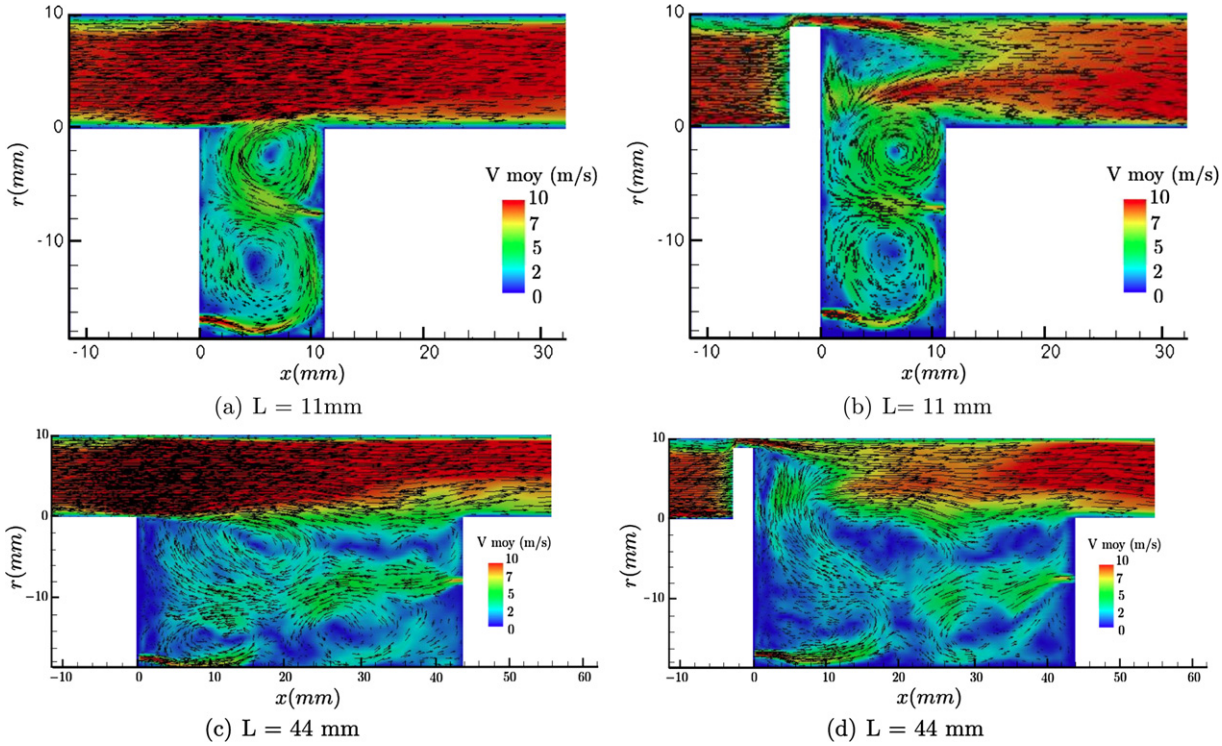

Fig. 8. Velocity magnitude. (a)–(c) Between rods; (b)–(d) behind a rod.

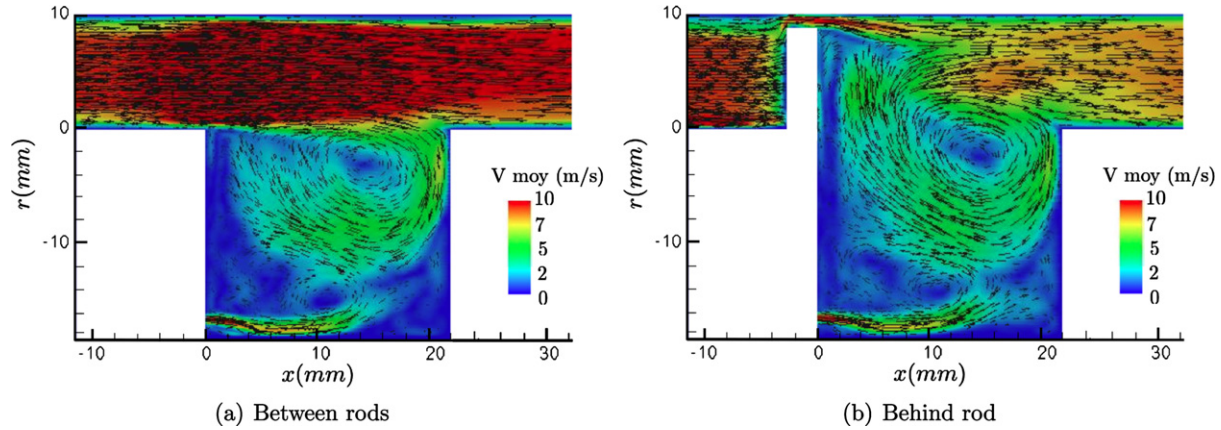

Fig. 9. Velocity magnitude without secondary-air injection.

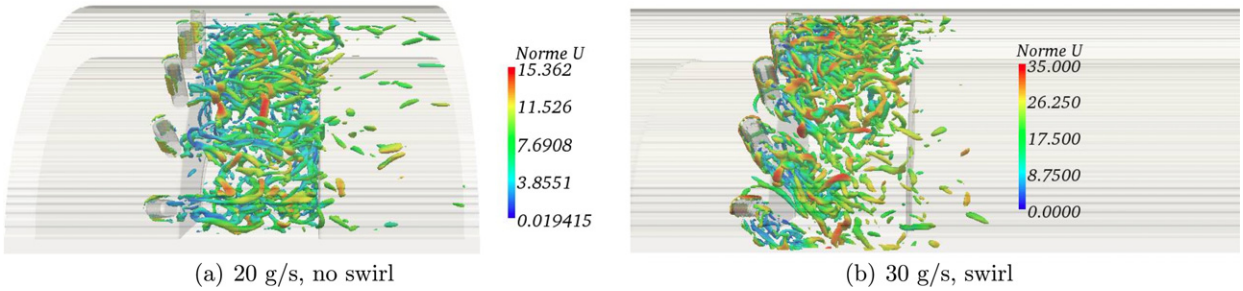

Fig. 10. Q-criterion ($Q = 9 \times 10^7\ s^{-2}$) colored by the velocity magnitude (m/s).

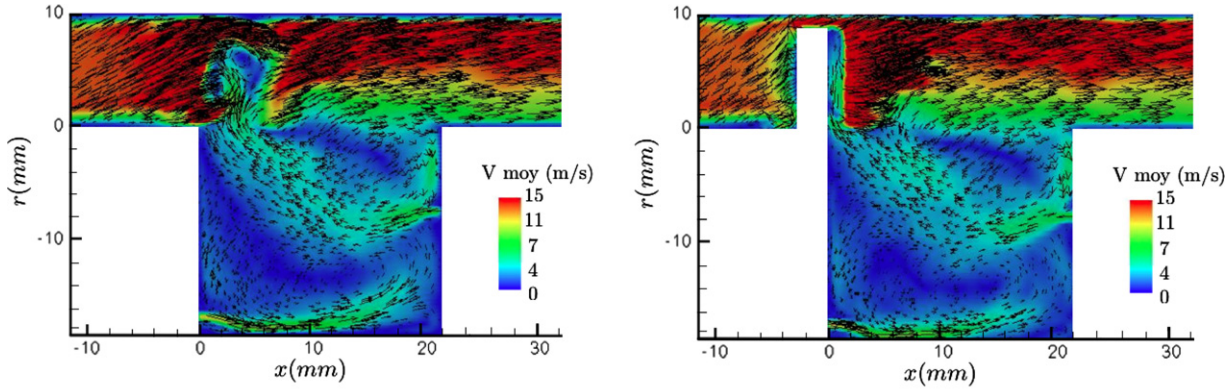

(a) Between rods (b) Between rods

Fig. 11. Velocity magnitude with swirled main annular flow.

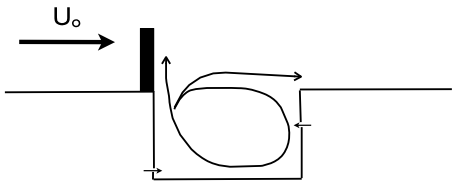

(a) Large flow rate

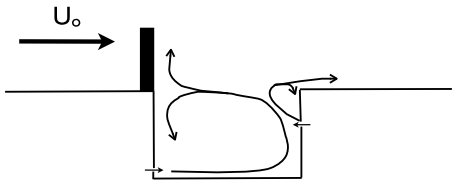

(b) Moderate flow rate

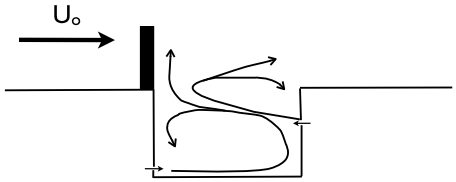

(c) Swirling flow

Fig. 12. Schematic of the cavity flow regimes.

in the cavity, which is then emptied by its upstream corner (Fig. 12(a)). This regime is of very limited interest, indeed in this particular case, flame stabilization should mainly result from a usual flame holder effect induced by the rods and the cavity would not play a major role. Decreasing the main flow velocity (about 20 g/s in the present experiment), a second unsteady vortex develops at the downstream corner, which is more or less amplified and coherent depending on the depth and length of the cavity (Fig. 12(b)); typically, the shorter the cavity length the stronger this secondary vortex. The shear layer is then very unsteady at the largest scales, with efficient fluid exchange between the main flow and the recirculating cavity motion. Adding swirl leads to an even more efficient mixing, with two strong main vortices and much fluid exchange between the cavity and the main flow (Fig. 12(c)).

4. Preserving flame speed in presumed-pdf modeling

In Large Eddy Simulation of turbulent flames, the sub-grid scale and unresolved transport by velocity fluctuations along with the impact of unresolved fluctuations of species and temperature on chemical reactions must be modeled. This has been addressed in the literature in many different ways [44]. For the chemical source in premixed turbulent combustion,

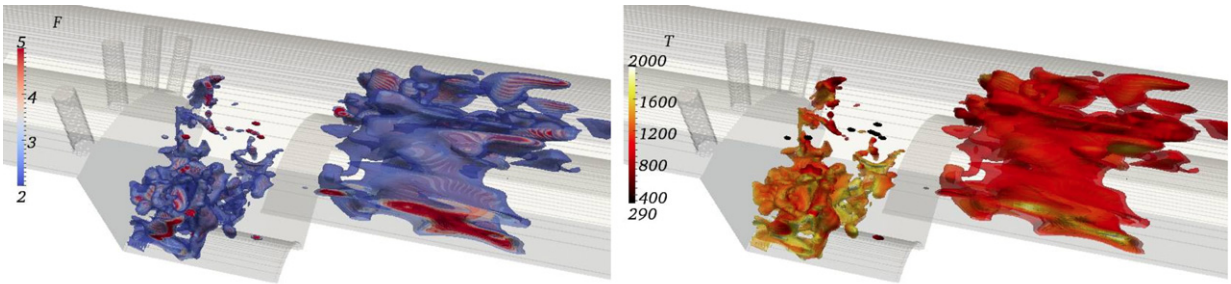

(a) F factor (Eq. (7)) (b) Temperature in Kelvin

Fig. 13. Iso-F and iso-temperature.

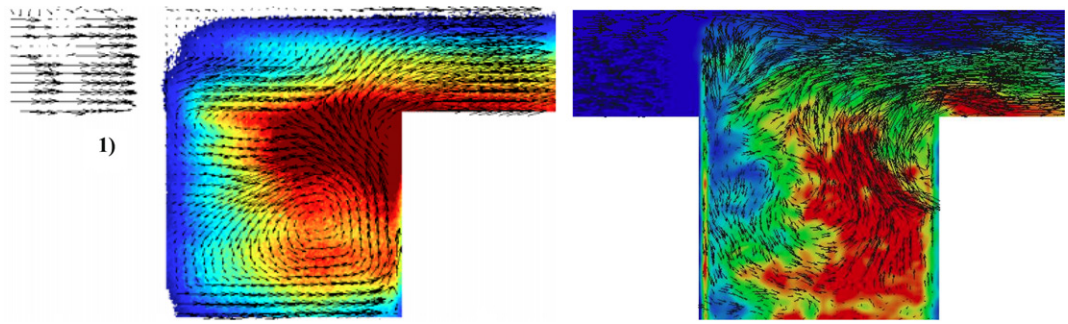

(a) $\theta = 49°$

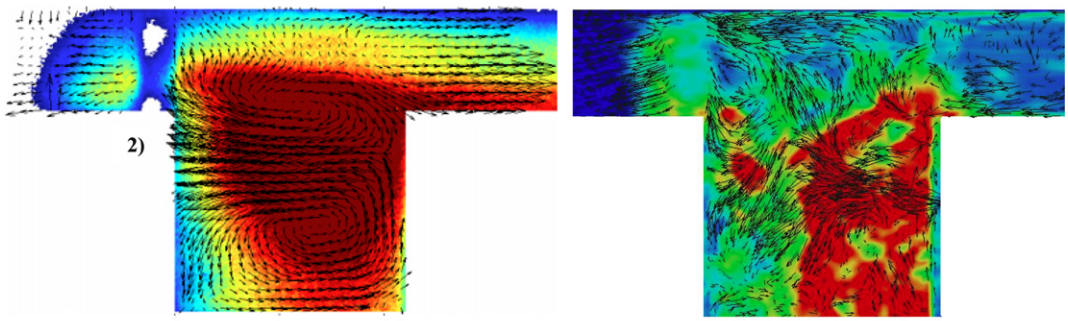

(b) $\theta = 109°$

Fig. 14. Left: CH* and PIV (2D). Right: LES. Baseline case (20 g/s).

one approach consists of tabulating chemistry from laminar flamelets using $Y_c(\xi, t)$, a progress of reaction defined versus ξ, a coordinate through the flame, so that all thermochemical quantities $\varphi(\xi, t)$ may be cast as a unique function of Y_c:

$$\varphi(\xi, t) = \varphi\big(Y_c(\xi, t)\big) \tag{1}$$

This trajectory in progress variable space is sometime called a 'manifold' and the corresponding tabulation technique Flame Generated Manifold [45] or FPI (Flame Prolongation of Intrinsic low-dimensional manifold) [46], methods which may also be extended to operate with more than a single parameter for the tabulation [47,48]. These approaches to downsize chemistry have been coupled with LES using various strategies, some based on presumed probability density function (pdf) of Y_c, or other parameters involved in the tabulation. Further details concerning the coupling between these methods and LES flow solvers may be found in [18,42,49,19,50,43].

A balance equation is solved for $\widetilde{Y}_c$, the filtered value of the progress of reaction, which takes the form with usual notations:

$$\frac{\partial \overline{\rho}\widetilde{Y}_c}{\partial t} + \nabla \cdot (\overline{\rho}\widetilde{\mathbf{u}}\widetilde{Y}_c) = \nabla \cdot \left(-\overline{\tau}_{Y_c} + \overline{\rho} D^*_{Y_c} \nabla \widetilde{Y}_c\right) + \widetilde{\dot{\omega}}_{Y_c} \tag{2}$$

$\overline{\rho}$ is the Reynolds space-filtered density, $\widetilde{\mathbf{u}}$ is the mass-weighted (or Favre) velocity vector, $\overline{\tau}_{Y_c} = \overline{\rho \mathbf{u} Y_c} - \overline{\rho}\widetilde{\mathbf{u}}\widetilde{Y}_c$ is the unresolved turbulent transport expressed, either with the Vreman closure [24] or set to zero in the case where MILES is

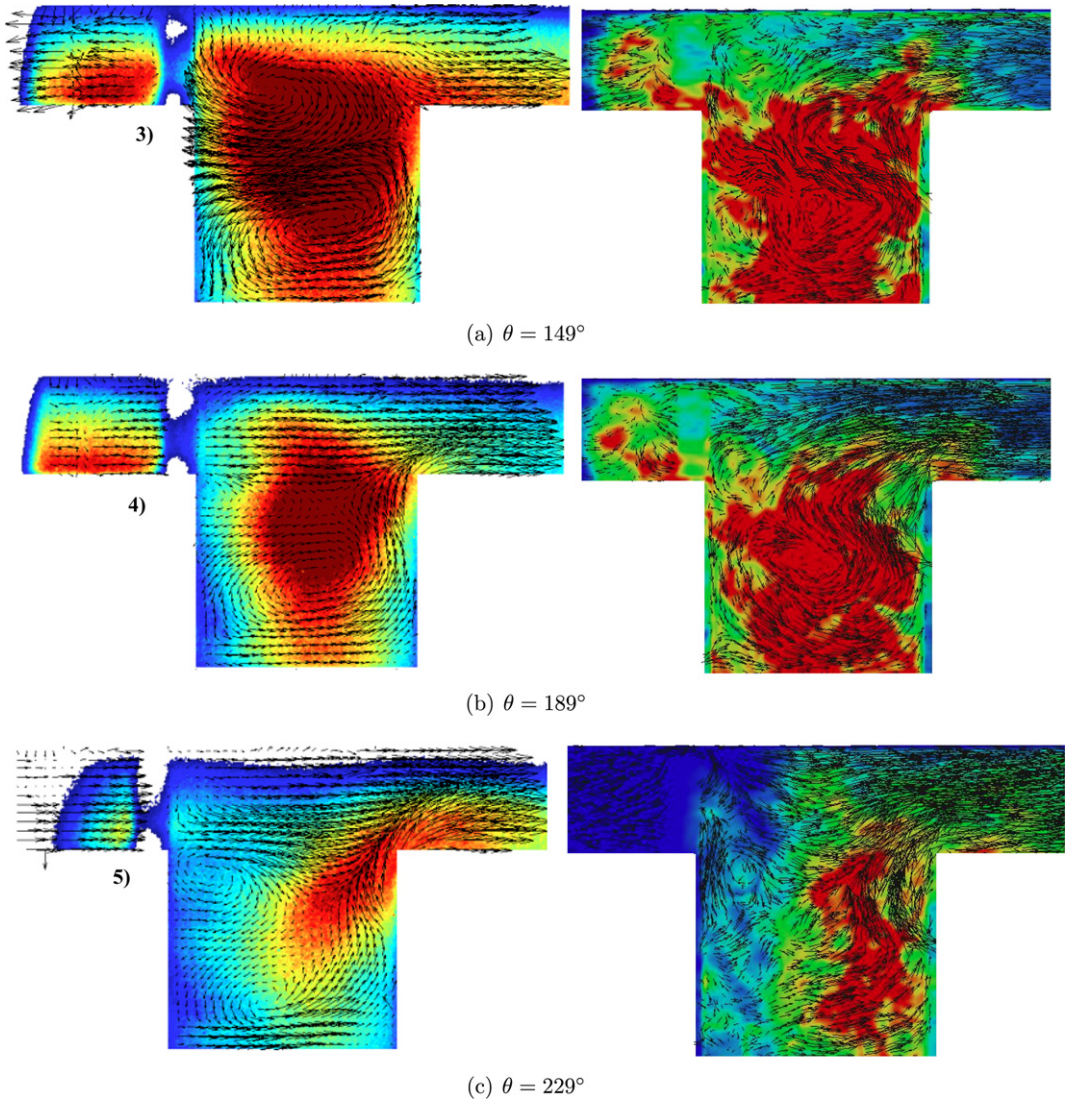

(a) $\theta = 149°$

(b) $\theta = 189°$

(c) $\theta = 229°$

Fig. 15. Left: CH* and PIV (2D). Right: LES. Baseline case (20 g/s).

adopted, as done here (see Section 2.2). $D^*_{Y_c}$ is a diffusion coefficient to be determined, and, $\widetilde{\dot{\omega}}_{Y_c}$ is the filtered chemical source computed with $\widetilde{P}(Y_c^+; \underline{x}, t)$, the presumed pdf [18]:

$$\widetilde{\dot{\omega}}_{Y_c}(\underline{x}, t) = \int_0^{Y_c^{Eq}} \dot{\omega}_{Y_c}\left(Y_c^+\right) \widetilde{P}\left(Y_c^+; \underline{x}, t\right) dY_c^+ \tag{3}$$

where Y_c^{Eq} is the equilibrium burnt gases value and $\dot{\omega}_{Y_c}(Y_c^+)$ is expressed from the flamelet tabulation (Eq. (1)). In practice, this pdf is parameterized with $\widetilde{Y}_c$ and the variance $Y_{c_v} = \widetilde{Y_c Y_c} - \widetilde{Y}_c \widetilde{Y}_c$, both obtained from balance equations [18], then the filtered burning rate becomes a simple function of $\widetilde{Y}_c$ and Y_{c_v}: $\widetilde{\dot{\omega}}_c = \widetilde{\dot{\omega}}_c(\widetilde{Y}_c, Y_{c_v})$; when $Y_{c_v} \to 0$, the flame is expected to be fully resolved over the mesh.

So far, in the simulations performed with such modeling, $D^*_{Y_c}$ was taken in a more or less arbitrary manner, for instance as the diffusion coefficient which provided the proper flame speed S_L for fully resolved laminar flame simulations performed under the constraint $Y_{c_v} = 0$ [42], to be subsequently applied for any level of SGS variance found in the turbulent flame. As done in the Thickened Flame LES (TFLES) approach [51], it is discussed how this diffusion coefficient should in fact be calibrated dynamically in the turbulent flame, here according to the local $\widetilde{Y}_c$ and Y_{c_v}.

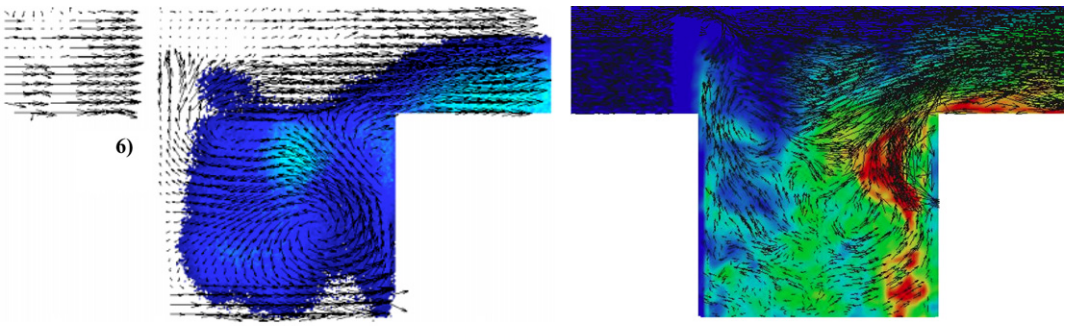

(a) $\theta = 289°$

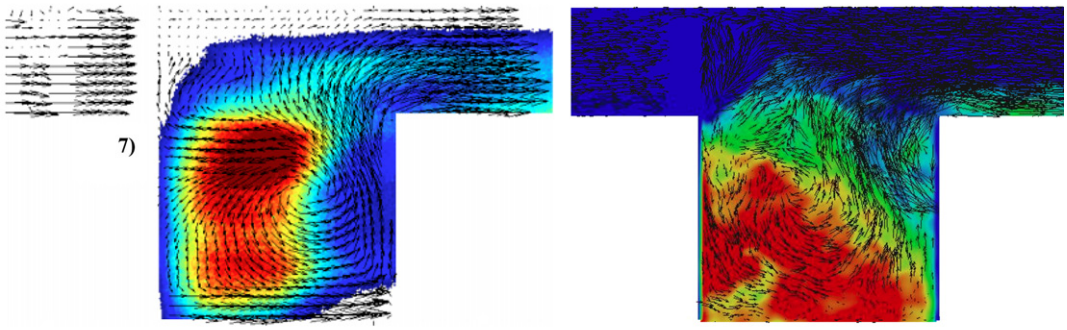

(b) $\theta = 349°$

Fig. 16. Left: CH* and PIV (2D). Right: LES. Baseline case (20 g/s).

In the one-dimensional and steady laminar reference flame, the Y_c budget reads:

$$\rho_o S_L \frac{dY_c}{d\xi} = \frac{d}{d\xi}\left(\rho D_{Y_c} \frac{dY_c}{d\xi}\right) + \dot{\omega}_{Y_c} \tag{4}$$

where ρ_o is the density in fresh gases, S_L is the laminar flame speed and D_{Y_c} the molecular diffusion coefficient, which may be computed from the species properties (for instance using Eq. (15) of [48]). The balance equation for $\widetilde{Y}_c$ should preserve some features of Eq. (4), as ensuring flame propagation at the correct speed and also capturing the proper order of magnitude of the flame thickness, a point that was also discussed in the case of a swirl burner and flame propagation after sparking in [52,53].

It is proposed in this article to determine the diffusion coefficient $D^*_{Y_c}$ of Eq. (2), so that the flame indeed propagates at a speed that tends towards S_L, either with the MILES approach or in flow zones where the modeling of $\overline{\tau}_{Y_c}$ returns low level of SGS eddy viscosity, *i.e.* highly resolved LES or weakly turbulent flame computed over a coarse mesh. As in the TFLES closure [51], let us consider a new coordinate $\xi^+ = F\xi$, with $F > 0$, then Eq. (4) becomes:

$$\rho_o S_L \frac{dY_c}{d\xi^+} = \frac{d}{d\xi^+}\left(\rho \mathcal{D}_{Y_c} \frac{dY_c}{d\xi^+}\right) + \dot{\Omega}_{Y_c} \tag{5}$$

with $\mathcal{D}_{Y_c} = F D_{Y_c}$ and $\dot{\Omega}_{Y_c} = \dot{\omega}_c / F$. The molecular diffusive coefficient $\mathcal{D}_{Y_c}$ preserving the flame speed may thus be written for any value of F:

$$\mathcal{D}_{Y_c} = \left(\frac{\dot{\omega}_c}{\dot{\Omega}_c}\right) D_{Y_c} \tag{6}$$

This shows that applying the factor $F = \dot{\omega}_c / \dot{\Omega}_c$ to the molecular diffusive coefficient used to compute the reference flame, ensures that the flame propagates at S_L, if $\dot{\omega}_c$ is the burning rate of the reference laminar flame and $\dot{\Omega}_c$ an expression used for modeling the burning rate over a coarse mesh. Within the context of above modeling, the burning rate of the laminar

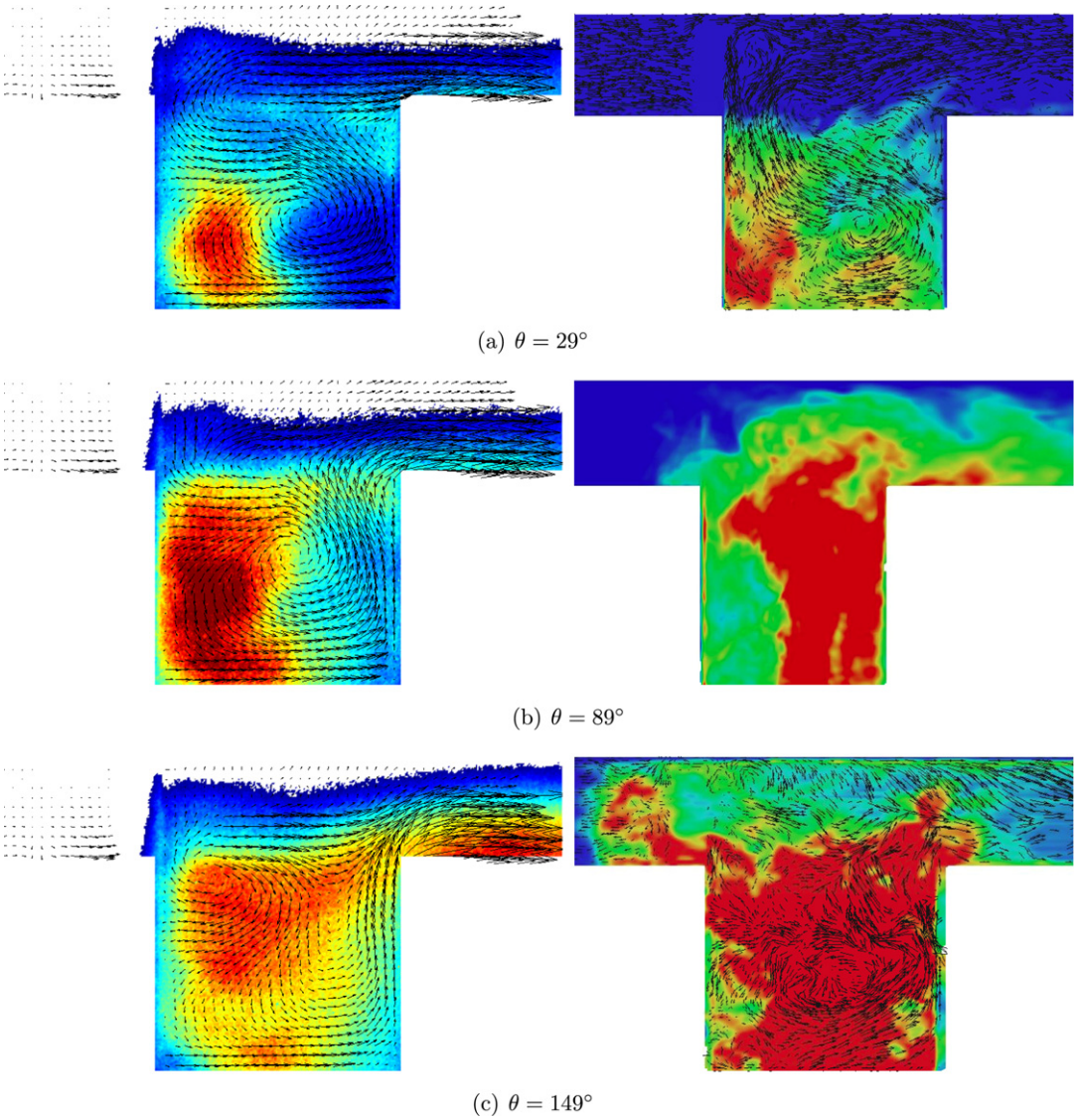

(a) $\theta = 29°$

(b) $\theta = 89°$

(c) $\theta = 149°$

Fig. 17. Left: CH* and PIV (2D). Right: LES. Swirling case (30 g/s).

flame is obtained setting the SGS variance Y_{c_v} to zero, then $F = \widetilde{\dot{\omega}}_c(\widetilde{Y}_c, Y_{c_v} = 0)/\widetilde{\dot{\omega}}_c(\widetilde{Y}_c, Y_{c_v})$. Therefore, $D^*_{Y_c}$ to be used in Eq. (2) for recovering the local flame speed in the turbulent simulation[1] reads:

$$D^*_{Y_c} = F D_{Y_c} = \left[\frac{\widetilde{\dot{\omega}}_c(\widetilde{Y}_c, Y_{c_v} = 0)}{\widetilde{\dot{\omega}}_c(\widetilde{Y}_c, Y_{c_v})}\right] D_{Y_c} \tag{7}$$

This last relation features strong similitudes with the TFLES approach [51], the present formulation may be seen as a thickening of the flame front with a dynamically computed thickening factor F that is determined from the variance, Y_{c_v}, convoluted with the chemical source response, $\widetilde{\dot{\omega}}_{Y_c}$, which does not take here the form of an Arrhenius law versus $\widetilde{Y}_c$ when Y_{c_v} is non-zero, as expected from DNS results [43]. The addition of a wrinkling factor [51] was not found necessary in the present simulations, this point may require further studies if the model is to be used with a very coarse mesh.

The relation (7) is used to simulate the Trapped Vortex Combustor with a beta-presumed pdf and a premixed flamelet tabulated chemistry, other details pertaining to this turbulent combustion closure may be found in [19]. The fully detailed methane–air mechanism GRI-3.0 [54] is used for building the chemical lookup table. Fig. 13 shows that F varies between 2 and 5 in the TVC simulations.

[1] Notice that this is only verified with no SGS transport, which is never exactly the case in LES, where physical or numerical SGS modeling impact on the actual propagation speed.

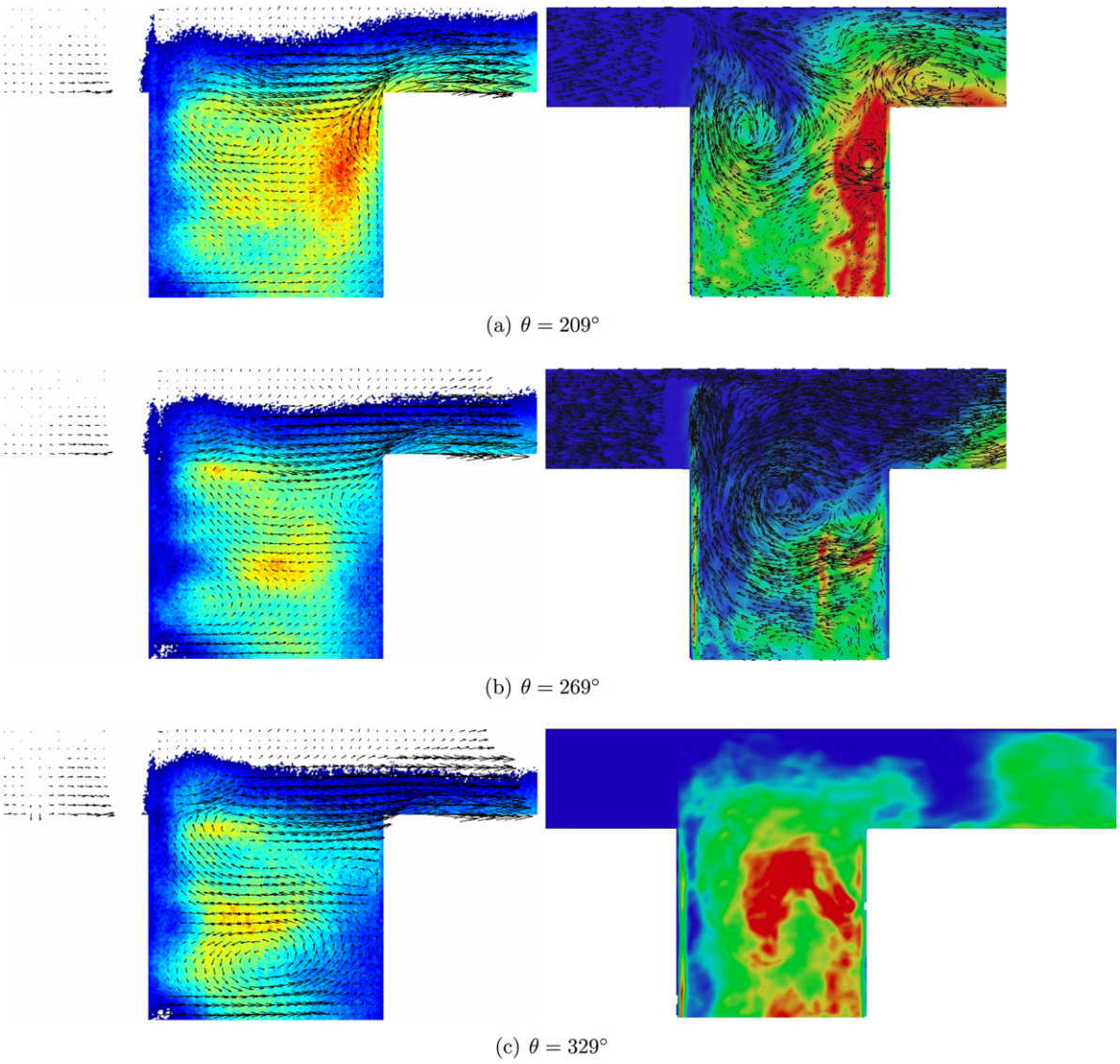

(a) $\theta = 209°$

(b) $\theta = 269°$

(c) $\theta = 329°$

Fig. 18. Left: CH* and PIV (2D). Right: LES. Swirling case (30 g/s).

5. Reactive TVC analysis

Flame structure was visualized in the experiment from CH* emission [16], collecting a signal that is spatially integrated, hence flame structure isolated in a given plane are out of reach at this stage. To mimic the measurements technique, maps of heat release rate have been averaged in LES over a set of planes in the azimuthal direction.

Figs. 14–16 show a typical sequence of the turbulent flame dynamics for the baseline case, as it was recorded both in the experiment and in the simulations; this sequence is decomposed into 7 stages in these figures according to a cycle of 360°. During this cycle, combustion first develops in the cavity, the recirculation zone is progressively filled out with burnt gases, hot gases expansion will then promote the transport of these gases downstream and the cycle can start again. The position $\theta = 40°$ in the cycle (Fig. 14(a)) is characterized by a flame located close to the downstream wall, with some weak flushing of the cavity at its downstream corner. At $\theta = 109°$ (Fig. 14(b)), the annular main flow is strongly perturbed, and fluid flows from the cavity in the vicinity of the rods. Then, at $\theta = 149°$ (Fig. 15(a)), the flame further develops to fill out all of the cavity, with some burning zone observed even upstream of flame holders. At $\theta = 189°$ (Fig. 15(b)), burning is still found upstream of the rods with enhanced cavity flushing by the downstream corner, then the flow is accelerated and the flame progressively leaves the cavity at $\theta = 229°$ (Fig. 15(c)), to end-up with almost no burning at $\theta = 289°$ (Fig. 15(a)); the cycle is then ready to resume at $\theta = 349°$ (Fig. 15(b)).

These results suggest that controlling the stability of combustion in the baseline case may not be that obvious; also following the cold flow study, the flame is now analyzed with the addition of a swirling motion in the main annular flow.

Figs. 17 and 18 show the experimental and simulated flame behavior with swirl. First, in opposition to the previous case, the burning zone mostly stays within the cavity, avoiding intermittent flash-back upstream of the flame holders. At $\theta = 29°$ (Fig. 17(a)), the flame is located close to the upstream wall, the flow cavity is decomposed into two main vortices, one in the bottom part of the cavity and the other in the shear layer. The bottom vortex growths to become a central and burning recirculation zone at $\theta = 89°$ (Fig. 17(b)). At $\theta = 149°$ (Fig. 17(c)), the flame is fully developed and starts to be convected downstream of the cavity; this process continues at $\theta = 209°$ (Fig. 18(a)), where the flame is close to the downstream cavity wall, with fresh fluid entering the cavity, to completely feed the cavity with reactants at $\theta = 269°$ (Fig. 18(b)); finally, a new flame kernel appears again at $\theta = 209°$ (Fig. 18(c)). Both experiment and simulation therefore provide an overall cycle that is much more encouraging in terms of overall flame stability; an observation confirmed by maximum pressure fluctuations recorded in the simulations and in the experiments of the order of 4000 Pa in the swirled case, against 10 000 Pa in the baseline one.

6. Summary

A trapped vortex burner has been discussed, analyzing results from Large Eddy Simulation compared against measurements. The Navier–Stokes equations are solved in their fully compressible form over a Cartesian grid, with immersed boundaries to capture the complex geometry including the cavity and an axisymmetric set of rods used as flame holders.

Three cavity flow modes have been reported, which controls the feeding of the cavity with reactants along with its flushing. The impact of varying the main flow rate, the cavity geometry and adding a swirl have been examined. The swirling case is found to be the best candidate for practical use of such burner, since it avoids strong pressure fluctuations resulting from the interaction of combustion with the cavity flushing modes.

In terms of sub-grid scale modeling, a novel strategy is proposed to calibrate dynamically the diffusion coefficient of the progress variable used in a presumed probability density function approach with premixed flamelets, in order to preserve the laminar flame speed value, over coarse meshes.

Acknowledgements

This work was granted access to the HPC resources of IDRIS-CNRS under the allocation 2011-020152 made by GENCI (Grand Equipement National de Calcul Intensif) and was funded by the European research project TECC-AE – FP7 (Technologies Enhancement for Clean Combustion in Aero-Engines), Grant No. 2010-020152 and by ANR (Agence Nationale de la Recherche) under the project ANR-10-LABX-09-01 (EMC3).

References

[1] T.Y.T. Wu, Cavity and wake flows, Annu. Rev. Fluid Mech. 4 (1972) 243–284.
[2] P.N. Shankar, M.D. Deshpande, Fluid mechanics in the driven cavity, Annu. Rev. Fluid Mech. 32 (2000) 93–136.
[3] B. Launder, S. Poncet, E. Serre, Laminar, transitional and turbulent flows in rotor–stator cavities, Annu. Rev. Fluid Mech. 42 (2010) 229–248.
[4] N. Forestier, L. Jacquin, P. Geffroy, The mixing layer over a deep cavity at high-subsonic speed, J. Fluid Mech. 475 (2003) 101–145.
[5] L. Larchevêque, P. Sagaut, O. Labbé, Large-eddy simulation of a subsonic cavity flow including asymmetric three-dimensional effects, J. Fluid Mech. 577 (2007) 105–126.
[6] E. Sanminguel-Rojas, J.I. Jiménez-González, P. Bohorquez, G. Pawlak, C. Martinez-Bazán, Effect of base cavities on the stability of the wake behind slender blunt-based axisymmetric bodies, Phys. Fluids 23 (11) (2011) 114103.
[7] B. Farkas, G. Paàl, K.G. Szabó, Descriptive analysis of a mode transition of the flow over an open cavity, Phys. Fluids 24 (2) (2012) 027102.
[8] K.-Y. Hsu, L.P. Goss, D.D. Trump, W.M. Roquemore, Performance of a Trapped-Vortex Combustor, AIAA Paper 0810.
[9] B.H. Little, R.R. Whipkey, Locked vortex afterbodies, J. Aircraft 16 (5) (1979) 296–302.
[10] R.C. Hendricks, R.C. Ryder, A. Brankovic, D.T. Shouse, W.M. Roquemore, N.-S. Liu, Computational parametric study of fuel distribution in an experimental trapped vortex combustor sector rig, in: Proceedings of ASME TURBO EXPO, vol. 1, ASME, 2004, pp. 81–92.
[11] M. Gharib, A. Roshko, The effect of flow oscillations on cavity drag, J. Fluid Mech. 177 (1987) 501–530.
[12] A. Roshko, K. Koenig, Interaction effects on the drag of bluff bodies in tandem, in: Aerodynamic Drag Mechanisms of Bluff Bodies and Road Vehicles, General Motors Research Laboratories, 1976.
[13] G.J. Sturgess, K.-Y. Hsu, Entrainment of mainstream flow in a Trapped-Vortex Combustor, AIAA Paper 0261.
[14] K.-Y. Hsu, L.P. Goss, W.M. Roquemore, Characteristics of a Trapped Vortex Combustor, J. Propulsion Power 14 (1) (1998) 57–65.
[15] J. Burguburu, Etude expérimentale de la stabilité d'une flamme dans une chambre de combustion aéronautique par recirculation de gaz brûlés et par ajout d'hydrogène, Ph.D. thesis, INSA de Rouen, 2011.
[16] J. Burguburu, G. Cabot, B. Renou, A. Boukhalfa, M. Cazalens, Flame stabilization by hot products gases recirculation in a trapped vortex combustor, in: ASME TURBO EXPO 2012 GT2012, Copenhagen, Denmark, June 11–15, 2012.
[17] W.M. Roquemore, D. Shouse, et al., Trapped vortex combustor concept for gas turbine engines, in: 39th AIAA Aerospace Sciences Meeting & Exhibit, AIAA 2001-0483, 2001, pp. 8–11.
[18] P. Domingo, L. Vervisch, D. Veynante, Large-eddy simulation of a lifted methane–air jet flame in a vitiated coflow, Combust. Flame 152 (3) (2008) 415–432.
[19] V. Subramanian, P. Domingo, L. Vervisch, Large-eddy simulation of forced ignition of an annular bluff-body burner, Combust. Flame 157 (3) (2010) 579–601.
[20] G. Lodato, L. Vervisch, P. Domingo, A compressible wall-adapting similarity mixed model for large-eddy simulation of the impinging round jet, Phys. Fluids 21 (2009) 035102.
[21] F. Ducros, F. Laporte, T. Soulères, V. Guinot, P. Moinat, B. Caruelle, High-order fluxes for conservative skew-symmetric-like schemes in structured meshes: Application to compressible flows, J. Comput. Phys. 161 (2000) 114–139.

[22] G. Lodato, P. Domingo, L. Vervisch, Three-dimensional boundary conditions for direct and large-eddy simulation of compressible viscous flows, J. Comput. Phys. 227 (10) (2008) 5105–5143.
[23] T. Poinsot, S.K. Lele, Boundary conditions for direct simulations of compressible viscous flows, J. Comput. Phys. 1 (101) (1992) 104–129.
[24] A.W. Vreman, An eddy-viscosity subgrid-scale model for turbulent shear flow: Algebraic theory and applications, Phys. Fluids 16 (10) (2004) 3670.
[25] P. Sagaut, Large Eddy Simulation for Incompressible Flows: An Introduction, 2nd edition, Springer-Verlag, Berlin, Heidelberg, 2001.
[26] A. Jameson, W. Schmidt, E. Turkel, Numerical solutions of the Euler equations by finite volume methods using Runge–Kutta time-stepping schemes, AIAA Paper 1259, 1981, p. 1981.
[27] R. Swanson, E. Turkel, On central-difference and upwind schemes, J. Comput. Phys. 101 (2) (1992) 292–306.
[28] S. Tatsumi, L. Martinelli, A. Jameson, Flux-limited schemes for the compressible Navier–Stokes equations, AIAA Journal 33 (2) (1995) 252–261.
[29] C. Merlin, P. Domingo, L. Vervisch, Immersed boundaries in large eddy simulation of compressible flows, Flow, Turbulence and Combustion, http://dx.doi.org/10.1007/s10494-012-9421-0, in press.
[30] M. Klein, A. Sadiki, J. Janicka, A digital filter based generation of inflow data for spatially developing direct numerical or large eddy simulations, J. Comput. Phys. 186 (2) (2002) 652–665.
[31] Y. Huang, V. Yang, Dynamics and stability of lean-premixed swirl-stabilized combustion, Progress in Energy and Combustion Science 35 (4) (2009) 293–364.
[32] C.D. Pierce, P. Moin, Large eddy simulation of a confined coaxial jet with swirl and heat release, in: 29th AIAA Fluid Dynamics Conference, AIAA 98-2892, Albuquerque, NM, June 15–18, 1998.
[33] D. Bradley, P.H. Gaskell, X.J. Gu, M. Lawes, M.J. Scott, Premixed turbulent flame instability and no formation in a lean-burn swirl burner, Combust. Flame 115 (4) (1998) 515–538.
[34] C. Stone, S. Menon, Swirl control of combustion instabilities in a gas turbine combustor, Proc. Combust. Inst. 29 (1) (2002) 155–160, http://dx.doi.org/10.1016/S1540-7489(02)80024-4.
[35] Y. Sommerer, D. Galley, T. Poinsot, S. Ducruix, S. Veynante, LES of flashback and extinction in a swirled burner, J. Turbulence 5 (1), http://dx.doi.org/10.1088/1468-5248/5/1/037.
[36] O. Stein, A. Kempf, J. Janicka, LES of the Sydney swirl flame series: An initial investigation of the fluid dynamics, Combust. Sci. Tech. 179 (2007) 173–189.
[37] A. Nauert, A. Dreizler, Conditional velocity measurements by simultaneously applied laser Doppler velocimetry and planar laser-induced fluorescence in a swirling natural gas/air flame, Z. Phys. Chem. 219 (2005) 635–648.
[38] C. Schneider, A. Dreizler, J. Janicka, Fluid dynamical analysis of atmospheric reacting and isothermal swirling flows, Flow, Turbulence and Combustion 74 (1) (2005) 103–127.
[39] S. Roux, G. Lartigue, T. Poinsot, U. Meier, C. Berat, Studies of mean and unsteady flow in a swirled combustor using experiments, acoustic analysis, and large eddy simulation, Combust. Flame 141 (1–2) (2005) 40–54.
[40] M. Freitag, M. Klein, DNS of a recirculating swirling flow and vortex breakdown, Flow, Turbulence and Combustion 1–4 (75) (2005) 51–66.
[41] W. Meier, P. Weigand, X. Duan, R. Giezendanner-Thoben, Detailed characterization of the dynamics of thermoacoustic pulsations in a lean premixed swirl flame, Combust. Flame 150 (1/2) (2007) 2–26.
[42] J. Galpin, A. Naudin, L. Vervisch, C. Angelberger, O. Colin, P. Domingo, Large-eddy simulation of a fuel lean premixed turbulent swirl burner, Combust. Flame 155 (1/2) (2008) 247–266.
[43] V. Moureau, P. Domingo, L. Vervisch, From large-eddy simulation to direct numerical simulation of a lean premixed swirl flame: Filtered laminar flame-pdf modeling, Combust. Flame 158 (7) (2011) 1340–1357.
[44] T. Poinsot, D. Veynante, Theoretical and Numerical Combustion, R.T. Edwards, Inc., 2005.
[45] J.A. van Oijen, F.A. Lammers, L.P.H. de Goey, Modeling of complex premixed burner systems by using flamelet-generated manifolds, Combust. Flame 127 (3) (2001) 2124–2134.
[46] O. Gicquel, N. Darabiha, D. Thevenin, Laminar premixed hydrogen/air counterflow flame simulations using flame prolongation of ILDM with differential diffusion, Proc. Comb. Inst. 28 (2000) 1901–1908.
[47] P. Nguyen, L. Vervisch, V. Subramanian, P. Domingo, Multidimensional flamelet-generated manifolds for partially premixed combustion, Combust. Flame 157 (1) (2010) 43–61, http://dx.doi.org/10.1016/j.combustflame.2009.07.008.
[48] G. Lodier, L. Vervisch, V. Moureau, P. Domingo, Composition-space premixed flamelet solution with differential diffusion for in situ flamelet-generated manifolds, Combust. Flame 158 (10) (2011) 2009–2016.
[49] J. Galpin, C. Angelberger, A. Naudin, L. Vervisch, Large-eddy simulation of H_2–air auto-ignition using tabulated detailed chemistry, J. of Turbulence 9 (13), http://dx.doi.org/10.1080/14685240801953048.
[50] N. Enjalbert, P. Domingo, L. Vervisch, Mixing time-history effects in large eddy simulation of non-premixed turbulent flames: Flow-controlled chemistry tabulation, Combust. Flame 159 (1) (2012) 336–352.
[51] O. Colin, F. Ducros, D. Veynante, T. Poinsot, A thickened flame model for large eddy simulations of turbulent premixed combustion, Phys. Fluids 12 (7) (2000) 1843–1863.
[52] G. Lecocq, S. Richard, O. Colin, L. Vervisch, Hybrid presumed pdf and flame surface density approach for large-eddy simulation of premixed turbulent combustion, part 1: Formalism and simulations of a quasi-steady burner, Combust. Flame 158 (6) (2011) 1201–1214.
[53] G. Lecocq, S. Richard, O. Colin, L. Vervisch, Hybrid presumed pdf and flame surface density approach for large-eddy simulation of premixed turbulent combustion, part 2: Early flame development after sparking, Combust. Flame 158 (6) (2011) 1215–1226.
[54] G.P. Smith, D.M. Golden, M. Frenklach, N.W. Moriarty, B. Eiteneer, M. Goldenberg, C.T. Bowman, R.K. Hanson, S. Song, W.C. Gardiner, V.V. Lissianski, Z. Qin, Tech. Rep., 1999, http://www.me.berkeley.edu/gri-mech/.